



# Analysis of temporal and spatial variability of atmospheric CO<sub>2</sub> concentration within Paris from the GreenLITE<sup>TM</sup> laser imaging experiment

Jinghui Lian<sup>1</sup>, François-Marie Bréon<sup>1</sup>, Grégoire Broquet<sup>1</sup>, T. Scott Zaccheo<sup>2</sup>, Jeremy Dobler<sup>3,a</sup>, Michel Ramonet<sup>1</sup>, Johannes Stauffer<sup>4,b</sup>, Diego Santaren<sup>1</sup>, Irène Xueref-Remy<sup>5,b</sup>, and Philippe Ciais<sup>1</sup>

<sup>1</sup>Laboratoire des Sciences du Climat et de l'Environnement (LSCE), IPSL, CEA-CNRS-UVSQ, Université Paris-Saclay, Gif-sur-Yvette, France

<sup>2</sup>Atmospheric and Environmental Research, Inc., Lexington, Massachusetts, USA

<sup>3</sup>Spectral Sensor Solutions LLC, Fort Wayne, Indiana, USA

<sup>4</sup>Thales, Labège, France

<sup>5</sup>Institut Méditerranéen de Biodiversité et d'Ecologie marine et continentale (IMBE), Aix Marseille Université, CNRS, IRD, Avignon Université, Aix-en-Provence, France

<sup>a</sup>formerly at: Harris Corporation, Fort Wayne, Indiana, USA

<sup>b</sup>formerly at: Laboratoire des Sciences du Climat et de l'Environnement (LSCE), IPSL, CEA-CNRS-UVSQ, Université Paris-Saclay, Gif-sur-Yvette, France

**Correspondence:** Jinghui Lian (jinghui.lian@lsce.ipsl.fr)

Received: 7 June 2019 – Discussion started: 4 July 2019

Revised: 2 October 2019 – Accepted: 11 October 2019 – Published: 18 November 2019

**Abstract.** In 2015, the Greenhouse gas Laser Imaging Tomography Experiment (GreenLITE<sup>TM</sup>) measurement system was deployed for a long-duration experiment in the center of Paris, France. The system measures near-surface atmospheric CO<sub>2</sub> concentrations integrated along 30 horizontal chords ranging in length from 2.3 to 5.2 km and covering an area of 25 km<sup>2</sup> over the complex urban environment. In this study, we use this observing system together with six conventional in situ point measurements and the Weather Research and Forecasting model coupled with Chemistry (WRF-Chem) and two urban canopy schemes (Urban Canopy Model – UCM; Building Effect Parameterization – BEP) at a horizontal resolution of 1 km to analyze the temporal and spatial variations in CO<sub>2</sub> concentrations within the city of Paris and its vicinity for the 1-year period spanning December 2015 to November 2016. Such an analysis aims at supporting the development of CO<sub>2</sub> atmospheric inversion systems at the city scale. Results show that both urban canopy schemes in the WRF-Chem model are capable of reproducing the seasonal cycle and most of the synoptic variations in the atmospheric CO<sub>2</sub> point measurements over the suburban areas as well as the general corresponding

spatial differences in CO<sub>2</sub> concentration that span the urban area. However, within the city, there are larger discrepancies between the observations and the model results with very distinct features during winter and summer. During winter, the GreenLITE<sup>TM</sup> measurements clearly demonstrate that one urban canopy scheme (BEP) provides a much better description of temporal variations and horizontal differences in CO<sub>2</sub> concentrations than the other (UCM) does. During summer, much larger CO<sub>2</sub> horizontal differences are indicated by the GreenLITE<sup>TM</sup> system than both the in situ measurements and the model results, with systematic east–west variations.

## 1 Introduction

Urban areas account for almost two-thirds of global energy consumption and more than 70 % of carbon emissions (IEA, 2008). Human activities, such as fossil fuel burning (Duren and Miller, 2012) and cement production (Wang et al., 2012), produce a net increase in atmospheric CO<sub>2</sub> concentration within and downwind of the emission sources. Over the

years, many instruments have been or will be used to measure the urban atmospheric CO<sub>2</sub> concentrations, including (i) ground-based monitoring networks in, e.g., Paris (Xueref-Remy et al., 2018), Indianapolis (Davis et al., 2017), Los Angeles (Feng et al., 2016), Washington, DC (Mueller et al., 2018), Boston (Sargent et al., 2018); (ii) airborne campaigns conducted in, e.g., Colorado (Graven et al., 2009), London (Font et al., 2015); (iii) existing space-based measurements, e.g., GOSAT (Hamazaki et al., 2004) and OCO-2 (Crisp et al., 2008; Crisp, 2015); and (iv) future satellites with imaging capabilities, e.g., OCO-3 (Elderling et al., 2019), GeoCarb (Moore et al., 2018), and CO2M (Buchwitz, 2018). These observations are used or could be used for estimating emissions of CO<sub>2</sub> over large cities using atmospheric inverse modeling or to detect emission trends if these data are collected over a sufficiently long period of time. High-accuracy continuous in situ ground-based measurements of CO<sub>2</sub> concentrations, using the cavity ring-down spectroscopy (CRDS) technology, have been used in previous urban atmospheric inversion studies for the quantification of CO<sub>2</sub> emissions of large cities (Bréon et al., 2015; Staufer et al., 2016; Lauvaux et al., 2016; Feng et al., 2016; Boon et al., 2016; Sargent et al., 2018). However, many in situ stations may be needed to accurately capture the CO<sub>2</sub> emission budget of a large city (Wu et al., 2016). Deploying such a network is expensive to install and maintain. The sparseness of CO<sub>2</sub> concentration sampling sites limits the ability of inversions to estimate the large spatial and temporal variations in the CO<sub>2</sub> emissions within the city, even though high-resolution emission inventories are available (e.g., AIRPARIF, 2013).

New concepts and technologies are desirable for a full sampling of atmospheric CO<sub>2</sub> concentrations within a city. These concepts may rely on moderate-precision but low-cost sensors that could be deployed at many sites for a high spatial density sampling (Wu et al., 2016; Arzoumanian et al., 2019). An alternative to in situ point measurements is a remote-sensing system based on the spectroscopic techniques which could provide long-path measurements of atmospheric trace gases over extended areas of interest. An example of this is the differential optical absorption spectroscopy (DOAS). It has been applied to monitor atmospheric air pollution such as nitrogen dioxide (NO<sub>2</sub>) and aerosol in a complex urban environment (Edner et al., 1993). A novel laser absorption spectroscopy based system for monitoring greenhouse gases was developed by Spectral Sensor Solutions LLC and Atmospheric and Environmental Research, Inc. (AER). This system, known as the Greenhouse gas Laser Imaging Tomography Experiment (GreenLITE<sup>TM</sup>), consists of a set of continuously operating laser-based transceivers and a set of retroreflectors separated by a few kilometers. Both data collection and data processing components are based on the intensity-modulated continuous-wave (IM-CW) measurement technique, which is described in detail in Dobler et al. (2017). This instrument provides estimates of the average CO<sub>2</sub> concentrations along the line of sight defined by the path be-

tween a laser-based transceiver and any given retroreflector. The path between a transceiver and a retroreflector is referred to as a “chord”. The GreenLITE<sup>TM</sup> system was developed and deployed as part of several field campaigns over the past several years (Dobler et al., 2013, 2017). These field tests have included extended operations at industrial facilities and have shown that the system is capable of identifying and spatially locating point sources of greenhouse gases (CO<sub>2</sub> and CH<sub>4</sub>) within a test area ( $\sim 1$  km<sup>2</sup>). In conjunction with the 21st Conference of Parties to the United Nations Framework Convention on Climate Change (COP 21), the GreenLITE<sup>TM</sup> system was deployed for a long-duration field test over central Paris, France. The objective was to demonstrate the potential of CO<sub>2</sub> concentration measurements along 30 horizontal chords ranging in length from 2.3 to 5.2 km and covering an area of 25 km<sup>2</sup>. The aim of this field campaign was to demonstrate the ability of GreenLITE<sup>TM</sup> to monitor the temporal and spatial variations in near-surface atmospheric CO<sub>2</sub> concentrations over the complex urban environment. In addition, these measurements may be used for post-deployment analysis of the CO<sub>2</sub> distribution with the ultimate goal of revealing the CO<sub>2</sub> emission distribution. As a first step, the objectives of this work are to assess the information content of the GreenLITE<sup>TM</sup> data, to analyze the atmospheric CO<sub>2</sub> distribution, and to characterize precisely the processes that lead to dilution and mixing of the anthropogenic emissions, which can provide new insights compared to the present in situ point measurement approaches due to a much wider spatial coverage.

The collection of the GreenLITE<sup>TM</sup> atmospheric CO<sub>2</sub> measurements in Paris makes it possible to evaluate and potentially improve meteorological and atmospheric transport models coupled to CO<sub>2</sub> emission inventories. On the other hand, the modeling system is expected to provide interpretations of the temporal and spatial variations in the GreenLITE<sup>TM</sup> data, with the aim of supporting the development of CO<sub>2</sub> atmospheric inversion systems at the city scale. Here we compare GreenLITE<sup>TM</sup> CO<sub>2</sub> data with simulations performed with the Weather Research and Forecasting Model coupled with a chemistry transport model (WRF-Chem). The WRF-Chem model allows various choices of physics parameterizations and data assimilation methods for constraining the meteorological fields (Deng et al., 2017; Lian et al., 2018). Previous studies have shown that it is necessary to account for specific urban effects when modeling the transport and dispersion of CO<sub>2</sub> over complex urban areas such as Salt Lake City, UT, and Los Angeles, CA (Nehrkorn et al., 2013; Feng et al., 2016). Nevertheless, even when the urban environment is accounted for, the modeling of atmospheric transport is a challenge. Significant mismatches remain between modeled and measured concentrations that could be explained by transport biases, particularly at night, and vertical mixing during the day.

In this study, we present the results from a set of 1-year simulations (from December 2015 to November 2016)

of CO<sub>2</sub> concentrations over the Paris megacity based on the WRF-Chem model coupled with two urban canopy schemes at a horizontal resolution of 1 km. The simulated CO<sub>2</sub> concentrations are compared with observations from the GreenLITE<sup>TM</sup> laser system as well as in situ CO<sub>2</sub> measurements taken continuously at six stations located within the Paris city limits and surrounding area. The detailed objectives of this paper are (i) to analyze in detail the information content of the GreenLITE<sup>TM</sup> data in addition to conventional in situ CO<sub>2</sub> measurements in order to better understand the temporal and spatial variations in near-surface CO<sub>2</sub> concentrations over Paris and its vicinity; (ii) to evaluate the performance of the high-resolution WRF-Chem model coupled with two urban canopy schemes (Urban Canopy Model – UCM; Building Effect Parameterization – BEP) for the transport of CO<sub>2</sub> over the Paris megacity area based on the two types of CO<sub>2</sub> measurements; (iii) to discuss the potential implications of assimilating the GreenLITE<sup>TM</sup> data into the CO<sub>2</sub> atmospheric inversion system with the ultimate goal of increasing the robustness of the quantification of city emissions and constraining the spatial distribution of the emissions within the urban area.

This paper is organized as follows. Sect. 2 provides more details about the GreenLITE<sup>TM</sup> deployment in conjunction with the in situ CO<sub>2</sub> monitoring network in Paris. The WRF-Chem modeling framework and model configurations are presented in Sect. 3. In Sect. 4, we evaluate the performance of the WRF-Chem simulations based on the analyses of the temporal and spatial patterns of observed and modeled CO<sub>2</sub> concentrations. Discussions and conclusions are given in Sect. 5.

## 2 The observation network

### 2.1 In situ measurements

Since 2010, a growing network of three to six in situ continuous CO<sub>2</sub> monitoring stations has been established in the Île-de-France (IdF) region in coordination with ongoing research projects (e.g., Bréon et al., 2015; Xueref-Remy et al., 2018). These observations are used to understand the variability of atmospheric CO<sub>2</sub> concentrations, with the aim to improve the existing bottom-up CO<sub>2</sub> emission inventories by providing a top-down constraint through atmospheric inverse modeling. The stations are equipped with high-precision analyzers for monitoring of atmospheric CO<sub>2</sub>, CO, and CH<sub>4</sub> installed on rooftops or towers to increase the area of representativity. All instruments have been regularly calibrated against the WMO cylinders (WMO–CO<sub>2</sub>–X2007 scale) (Tans et al., 2011).

The locations of the stations are given in Table 1a and are shown in Fig. 1a. Four stations are located within the peri-urban area: the OVS site is located about 26 km southwest of central Paris with a sampling height of 20 m a.g.l. (above the ground level) on the top of a building. The SAC tall

tower is located on the Plateau de Saclay (9.5 km southeast of OVS) with two air inlets placed at 15 m and 100 m a.g.l. The other two sites are located at the north (AND) and north-east (COU) edges of the Paris urban area in a mixed urban–rural environment with single inlets at 60 m and 30 m a.g.l. These four peri-urban stations are complemented by in situ continuous measurements at two urban stations: one at the Cité des Sciences et de l’Industrie (CDS) and one at the former Pierre and Marie Curie University (now Sorbonne University, also called Jussieu; JUS). The inlets for each of the sensors are placed at approximately 34 m and 30 m a.g.l. The JUS station is on the roof of a building close to ventilation outlets and may be influenced by this and other localized sources of CO<sub>2</sub>. The JUS site was only measuring CO<sub>2</sub> continuously from January to April 2016 and from 16 September 2016 through the end of this study. The spatial distribution of the monitoring sites was chosen a priori to best enable the analysis of gradients due to emissions in Paris when the wind is blowing from either the southwest or northeast directions, which corresponds to the prevailing winds in the region (Bréon et al., 2015; Staufer et al., 2016; Xueref-Remy et al., 2018).

### 2.2 The GreenLITE<sup>TM</sup> campaign over Paris

The GreenLITE<sup>TM</sup> system was deployed in Paris in November 2015 as a proof-of-concept demonstration during the COP 21 conference, and kept operating for 1 year. This system used two transceivers coupled with 15 retroreflectors to measure the CO<sub>2</sub> concentrations along 30 intertwined lines (chords) of 2.3–5.2 km length covering an area of 25 km<sup>2</sup> over the center of Paris. Each transceiver used two fiber-coupled distributed feedback lasers to generate an absorption line at a wavelength of 1571.112 nm and an off-line wavelength with significantly lower absorptions (nominally 1571.061 nm). The experimental design and layout examined in this study are given in Table 1b and are illustrated in Fig. 1b. The two transceivers were located on two rooftops: one on the lower of the two Montparnasse buildings (T1) (50.3 m a.g.l.) and the other on the Jussieu tower (T2) (86.8 m a.g.l.) located near the JUS in situ instrument. These locations were chosen based on a clear line of sight to the retroreflectors which were installed on additional rooftops around the city with heights varying from 16.8 to 50.4 m a.g.l. For this implementation, each transceiver scanned the retroreflectors in sequence and made a transmission measurement of each chord with a period of 4 min. The experiment lasted from November 2015 to November 2016 with some sporadic downtime of either the transceivers and/or some of the reflectors.

Preliminary analysis shows that the original GreenLITE<sup>TM</sup> CO<sub>2</sub> concentrations have a slow drift of approximately  $\pm 5$  ppm in comparison to both the nearby in situ measurements (Fig. S1 in the Supplement) and simulations with the CHIMERE transport model driven by operational forecasts

**Table 1.** Information about CO<sub>2</sub> observation stations used in this study.

(a) In situ stations																
Site		Abbreviation	Latitude (°)	Longitude (°)	Height (m a.g.l.)											
Jussieu		JUS	48.8464	2.3561	30											
Cité des Sciences et de l'Industrie		CDS	48.8956	2.3880	34											
Andilly		AND	49.0126	2.3018	60											
Coubron		COU	48.9242	2.5680	30											
Observatoire de Versailles Saint-Quentin-en-Yvelines		OVS	48.7779	2.0486	20											
Saclay		SAC	48.7227	2.1423	15 and 100											

(b) The GreenLITE™ system																
		R01	R02	R03	R04	R05	R06	R07	R08	R09	R10	R11	R12	R13	R14	R15
Chord length (km)	T1	2.80	2.67	3.17	4.02	3.81	4.84	4.59	4.53	5.06	4.72	4.88	4.93	4.94	4.93	4.71
	T2	5.11	4.91	5.00	5.17	4.30	5.00	4.59	4.38	4.28	3.40	3.37	3.30	2.90	2.74	2.39
Height (m a.g.l.)	R	50.4	41.7	18.3	28.1	19.7	20.8	24.5	25.9	16.9	28.8	29.7	24.7	21.8	16.8	23.6
	T	T1: 50.3; T2: 86.8														

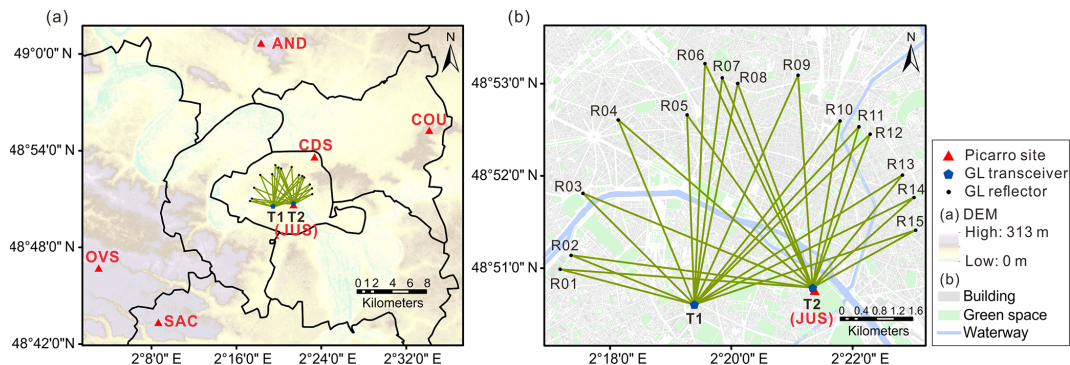


**Figure 1.** (a) Distribution of in situ CO<sub>2</sub> measurements and the GreenLITE™ laser system. The city of Paris is located within the inner line, but the urban area extends over a larger surface, very roughly within the Greater Paris area (including Paris and the three administrative areas that are around Paris called “Petite Couronne” in French; see Fig. S5). The Île-de-France region covers an area that is larger than the domain shown here. (b) The GreenLITE™ laser system layout and its chord labels. Data sources: the ASTER global digital elevation model (GDEM) Version 2 data are available at <https://lpdaac.usgs.gov/products/astgtmv002/> (last access: 12 November 2019); the administrative division map of the Île-de-France region is available at <https://www.data.gouv.fr/en/datasets/geofla-departements-idf/> (last access: 12 November 2019) and is the same for Figs. 2, 4, and S5; the building, green space, and waterway information are from OpenStreetMap (© OpenStreetMap contributors 2019, distributed under a Creative Commons BY-SA License.) available at <http://download.geofabrik.de/europe/france/ile-de-france-190907-free.shp.zip> (last access: 9 September 2019).

from ECMWF using the model configurations that are presented in Staufer et al. (2016). These slowly time-varying differences were most likely due to a slight systematic long-term drift in both the on- and off-line wavelengths as a function of continuous operations. Such drift may induce some nonlinear impacts on the measured concentrations. It is therefore more appropriate to adjust the wavelengths rather than to apply a linear calibration to the retrieved concentrations. Unlike in situ point measurement systems, there is no established method for calibration of long open-path systems to the WMO mole fraction scale used as an international standard for atmospheric CO<sub>2</sub> monitoring (Tans et al., 2011).

Therefore, a bias correction method was developed by AER (Zaccheo et al., 2019) for addressing observed slowly drifting biases between the GreenLITE™ prototype system and the two in situ sensors (CDS and JUS) that are near the GreenLITE™ chords. This method computed a time-varying adjustment to the off-line wavelength based on a nonlinear optimization mechanism. This nonlinear approach adjusts the GreenLITE™ off-line wavelength considering not only the average values of hourly CO<sub>2</sub> concentrations at two in situ stations, but also the corresponding average temperature, relative humidity, atmospheric pressure along the chord, and an optimized online wavelength value during the mea-

surement period. Finally, the median on- and off-line values over a 4 d window were used to recompute the GreenLITE<sup>TM</sup> data from all chords using a radiative-transfer-based iterative retrieval scheme based on the line-by-line radiative transfer model (Clough et al., 2005). Even though this approach is not ideal as the two in situ stations and the GreenLITE<sup>TM</sup> system do not sample the exact same area, it does provide a well-defined mechanism that reduces the systematic long-term biases with no significant impact on the chord-to-chord variations. Top panels in Fig. S2a and b show the distribution of the absolute values of the daily averaged CO<sub>2</sub> concentration difference between all pairs of chords for each transceiver before and after the calibration. The differences between the medians of the re-processed and original inter-chord range, shown in bottom panels in Fig. S2a and b, are within in the range of  $\pm 0.5$  ppm for T1 and  $\pm 2$  ppm for T2 with the respective yearly mean plus/minus 1 standard deviation of  $0.04 \pm 0.16$  ppm for T1 and  $0.48 \pm 0.43$  ppm for T2.

In order to enable the data to be compared to hourly in situ observations and WRF-Chem outputs, hourly means are computed from the 4 min GreenLITE<sup>TM</sup> data after applying the calibration approach described above. Two additional selection criteria were also established for this work: (i) a minimum of three valid 4 min samples were necessary to generate a valid hourly average for a given chord, and (ii) the standard deviation of these samples had to be smaller than 10 ppm. The 10 ppm threshold was selected to be roughly 3 times the typical standard deviation of the 4 min measurements for any given chord within a 1 h period (Fig. S3). Data that do not meet the above criteria, about 1.06 % of the total, were considered invalid and excluded from further analysis.

### 3 Modeling framework

#### 3.1 WRF-Chem model setup

A set of high-resolution simulations of atmospheric CO<sub>2</sub> concentrations was performed with WRF-Chem V3.9.1 on-line coupled with the diagnostic biosphere Vegetation Photosynthesis and Respiration Model (VPRM) (Mahadevan et al., 2008; Ahmadv et al., 2007, 2009). The simulations were carried out over the period spanning September 2015 to November 2016, in which the first 3 months were regarded as a spin-up period. Three one-way nested domains were employed with the horizontal grid resolution of 25, 5, and 1 km, covering Europe (Domain 01), Northern France (Domain 02), and the IdF region (Domain 03), respectively (Fig. S4). The meteorological initial and lateral boundary conditions were imposed using the ERA-Interim global re-analyses with  $0.75^\circ \times 0.75^\circ$  horizontal resolution and 6-hourly intervals (Berrisford et al., 2011). We nudged the 3-D fields of temperature and wind to the ERA-Interim reanalysis in layers above the planetary boundary layer (PBL) of the outer two domains using the grid nudging option in WRF.

We also assimilated observation surface weather station data (ds461.0) and upper-air meteorological fields (ds351.0) from the Research Data Archive at the National Center for Atmospheric Research (<https://rda.ucar.edu/datasets/ds351.0/>, last access: 12 November 2019; <https://rda.ucar.edu/datasets/ds461.0/>, last access: 12 November 2019) using a nudging technique (the surface analysis nudging and observation nudging options of WRF are described in detail in Lian et al., 2018). Details regarding the model configurations used in this study are summarized in Table 2.

The urban canopy parameterization is a critical element in reproducing the lower boundary conditions and thermal structures, which are of vital importance for accurate modeling of the transport and dispersion of CO<sub>2</sub> within the urban areas. We therefore paid special attention, in this study, to examining the impact of the two available urban canopy schemes on WRF-Chem transport results, namely the single-layer UCM (Chen et al., 2011) and the multilayer urban canopy model BEP (Martilli et al., 2002). This study does not assess the multilayer urban parameterization BEP+BEM (BEP combined with the Building Energy Model, BEM) (Salamanca et al., 2010) since this parameterization focuses on the impact of heat emitted by air conditioners, which are not commonly used in Paris. This study used 34 vertical layers in WRF-UCM with the top model pressure set at 100 hPa, and 15 layers arranged below 1.5 km with the first layer top at approximately 19 m a.g.l. In order to take full advantage of the WRF-BEP configuration, it is necessary to have a fine discretization of the vertical levels close to the surface. This configuration with 44 vertical layers, places 25 of them within the lowest 1.5 km, with the lowest level being around 3.8 m a.g.l. In order to select an adequate model physical configuration for Paris, we carried out some preliminary sensitivity experiments to test the impact of different physical schemes on the simulated CO<sub>2</sub> concentrations. These tests use up to five different PBL schemes and two urban canopy schemes. The simulations were carried out for 2 months: 1 winter month (January 2016) and 1 summer month (July 2016). These preliminary sensitivity results indicate that different PBL schemes in the WRF-Chem model lead to monthly average differences of 2–3 ppm on the simulated CO<sub>2</sub> concentrations over Paris, whereas the two different urban canopy schemes lead to much larger differences of 8–10 ppm. Thus in this study, we carried out the 1-year simulation with two different urban canopy schemes as they are sufficient to address the paper's main question regarding the ability of a configuration of the WRF-Chem model to simulate the CO<sub>2</sub> atmospheric transport in an urban environment, but also to provide an estimate of the modeling uncertainty. All of the other physics options remained the same for the two experiments (Table 2): the WRF Single Moment 6-class (WSM6) microphysics scheme (Hong and Lim, 2006), the Rapid Radiative Transfer Model (RRTM) longwave radiation scheme (Mlawer et al., 1997), the Dudhia shortwave radiation scheme (Dudhia, 1989), the Mellor–Yamada–Janjić

**Table 2.** A summary of WRF-Chem configurations used in this study.

Option		Setting
Simulation periods		1 September 2015–30 November 2016
Horizontal resolution		25 km (Domain 01), 5 km (Domain 02), 1 km (Domain 03)
Boundary and initial conditions	Meteorology	ERA-Interim reanalysis data ( $0.75^{\circ} \times 0.75^{\circ}$ , 6-hourly)
	CO <sub>2</sub> concentration	LMDZ_CAMS ( $3.75^{\circ} \times 1.895^{\circ}$ , 3-hourly)
Nudging		Grid nudging + surface nudging + observation nudging (NCEP operational global observation surface data (ds461.0) and upper-air data (ds351.0))
Flux	Anthropogenic emissions	IER inventory for 2005 (5 km, outside IdF) + AIRPARIF inventory for 2010 (1 km, within IdF) rescaled for 2015–2016 using national budgets from Le Quéré et al. (2018)
	Biogenic NEE	VPRM (online coupling)
Physics schemes	Microphysics	WSM6 scheme
	Cumulus convection	Grell 3-D ensemble scheme only in Domain 01
	Longwave radiation	RRTM scheme
	Shortwave radiation	Dudhia scheme
	PBL	MYJ scheme
	Surface layer	Eta Similarity scheme
	Vegetated land surface	Unified Noah land-surface model
	Urban land surface	UCM (34 vertical levels, wherein 15 are below 1.5 km)
		BEP (44 vertical levels, wherein 25 are below 1.5 km)

(MYJ) PBL scheme (Janjić, 1990, 1994), the Eta Similarity surface layer scheme (Janjić, 1996), and the Unified Noah land-surface scheme (Chen and Dudhia, 2001). The Grell 3-D ensemble cumulus convection scheme (Grell and Dévényi, 2002) was applied for Domain 01 only in both experiments.

## 3.2 CO<sub>2</sub> simulations

### 3.2.1 Anthropogenic CO<sub>2</sub> fluxes

Anthropogenic CO<sub>2</sub> fluxes within the IdF region are imposed using the AIRPARIF inventory for the year 2010 at spatiotemporal resolutions of 1 km and 1 h (AIRPARIF, 2013). This inventory is based on various anthropogenic activity data, emission factors and spatial distribution proxies, which are described in detail in Bréon et al. (2015). It provides maps and diurnal variations for 5 typical months (January, April, July, August, and October) and 3 typical days (a weekday, Saturday, and Sunday) to account for the seasonal, weekly and diurnal cycles of the emissions (see Fig. 3 in Bréon

et al., 2015). CO<sub>2</sub> emissions from fossil fuel CO<sub>2</sub> sources outside the IdF region are taken from the inventory of the European greenhouse gas emissions, together with country-specific temporal profiles (monthly, daily, and hourly) at a spatial resolution of 5 km (updated in October 2005). This inventory was developed by the Institute of Economics and the Rational Use of Energy (IER), University of Stuttgart, under the CarboEurope-IP project (<http://www.carboeurope.org/>, last access: 12 November 2019).

Both inventories are adapted to the WRF-Chem model for the period of simulation (September 2015–November 2016). Moreover, we scale these two data sets to account for annual changes in emission between the base years and simulation timeframe. This is accomplished by rescaling the maps with the ratio of the annual budgets of national CO<sub>2</sub> emissions for the countries within the domain between the base year 2005 for IER and 2010 for AIRPARIF and the year of simulation (2015/2016), taken from Le Quéré et al. (2018) (<https://www.icos-cp.eu/GCP/2018>, last access: 12 Novem-



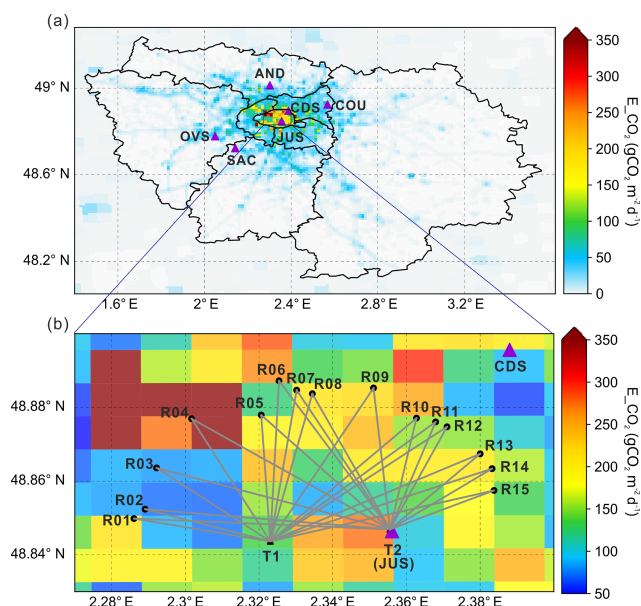


**Figure 2.** Total CO<sub>2</sub> emissions, according to the AIRPARIF inventory (within IdF) and the IER inventory (outside IdF), for a weekday in March 2016. Panel (a) shows the CO<sub>2</sub> emissions over the IdF region together with the in situ measurement stations. Panel (b) is a high-resolution zoom of the inner Paris area and shows the 1 km emissions together with the GreenLITE<sup>TM</sup> chords and two urban in situ measurement stations.

ber 2019). See also Table S1 in the Supplement for details about original data sources). Finally, we interpolate the emissions onto the WRF-Chem grids, making sure to conserve the total budget of emission in the process, as done in previous studies (e.g., Ahmadov et al., 2007). Note that for the point sources such as stacks, industries, and mines, CO<sub>2</sub> emissions are distributed over a single grid cell corresponding to their locations. Figure 2 shows the spatial distribution of the total CO<sub>2</sub> emissions for a weekday in March over the IdF region at the resolution of 1 km × 1 km. It can be seen that there is a large spatial variability of CO<sub>2</sub> emissions ranging from 0 to more than 600 g CO<sub>2</sub> m<sup>-2</sup> d<sup>-1</sup> in this area and the largest emissions are concentrated over the Greater Paris area, accounting for about 50 % of the emitted CO<sub>2</sub>.

Based on the analysis of sectorally specific fossil fuel CO<sub>2</sub> emissions over the IdF region by Wu et al. (2016), we group the detailed sectoral AIRPARIF emissions into five main sectors, namely building (43 %), energy (14 %), surface traffic (29 %), aviation-related surface emissions (4 %), and all other sectors (10 %), where the percentages in parenthesis express the relative contribution of each sector to the yearly total. All emissions are injected in the first model layer. Distinct CO<sub>2</sub> tracers are used for each of the five main sectors in the transport model to record their distinct CO<sub>2</sub> atmospheric signature. Figure 3 shows averages at the monthly scale of emissions below the GreenLITE<sup>TM</sup> chords for those different sectors. It illustrates that CO<sub>2</sub> emissions have a large seasonal

cycle, mostly due to the residential heating (the “building” sector) which is strongly driven by variations in the atmospheric temperature. Figure 3 also reveals lower emissions for those chords (TX and R01-03) in the west of Paris than those in the other quadrants.

### 3.2.2 Biogenic CO<sub>2</sub> fluxes

Biogenic CO<sub>2</sub> fluxes are simulated with the VPRM model forced by meteorological fields simulated by WRF and online-coupled to the atmospheric transport. VPRM uses the simulated downward shortwave radiation and surface temperatures, along with the vegetation indices (enhanced vegetation index and land surface water index) derived from the 8 d MODIS Surface Reflectance Product (MOD09A1) and four parameters for each vegetation category (PAR0, λ, α, β) that are optimized against eddy covariance flux measurements over Europe collected during the Integrated EU project “CarboEurope-IP” (<http://www.carboeurope.org/>, last access: 12 November 2019). The land cover data used by VPRM (see Fig. S5) are derived from the 1 km global Synergetic Land Cover Product (SYNMAP; Jung et al., 2006) reclassified into eight different vegetation classes (Ahmadov et al., 2007, 2009).

Figure 4a shows the spatial distribution of daytime-averaged (06:00–18:00 UTC) CO<sub>2</sub> biogenic flux (the net ecosystem CO<sub>2</sub> exchange, hereafter NEE, with a negative sign indicating net CO<sub>2</sub> uptake by the vegetation surface) in June 2016. The model simulates negative values of NEE (uptake of more than 5 g CO<sub>2</sub> m<sup>-2</sup> d<sup>-1</sup>) over most of the region with the exception in urban areas where the values are assigned to 0. Figure 4b shows the mean diurnal cycles of NEE for 12 calendar months and for eight vegetation classes used in VPRM over Domain 03. The magnitude of NEE is highly dependent on the vegetation types, although the diurnal cycles are similar across these vegetation types. From November to January, the VPRM estimates within the IdF region show a small diurnal cycle and a positive NEE explained by ecosystem respiration exceeding gross primary productivity. One exception to positive wintertime NEE is for evergreen trees which, according to the VPRM model, sustain enough gross primary productivity to keep a negative daytime NEE throughout the year. The model shows large CO<sub>2</sub> uptake between late spring and early summer. Note that the seasonal cycle of crops, which dominates over the IdF region, is somewhat different from that of forests, with an NEE that decreases after the harvest in June/July; this crop phenology signal is being driven by the MOD09A1 data. Grasses also have a shorter uptake period than the other vegetation types, with a positive NEE as early as August.

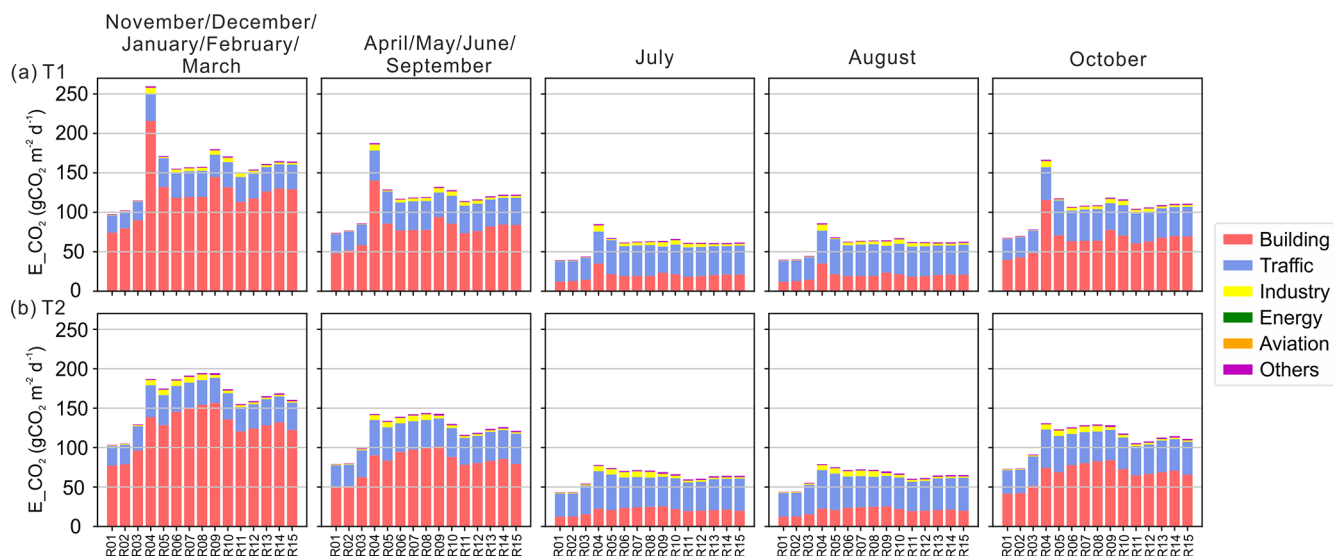


**Figure 3.** Averaged anthropogenic CO<sub>2</sub> fluxes along each GreenLITE™ chord according to the AIRPARIF inventory.

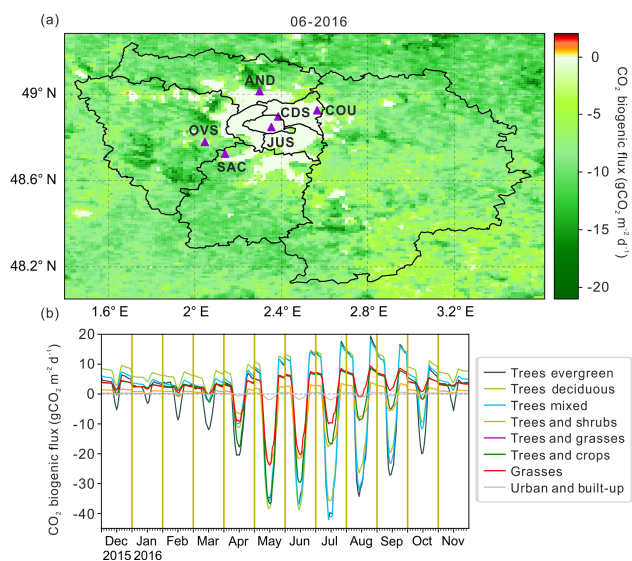


**Figure 4.** (a) Daytime (06:00–18:00 UTC) average of CO<sub>2</sub> biogenic flux (NEE) in June 2016; (b) mean diurnal cycles of CO<sub>2</sub> biogenic flux (NEE) for 12 calendar months and for eight vegetation classes used in VPRM over Domain 03.

### 3.2.3 Initial and lateral boundary conditions for CO<sub>2</sub>

Initial and lateral boundary conditions for CO<sub>2</sub> concentration fields used in the WRF-Chem model are taken from the 3-hourly fields of the CAMS global CO<sub>2</sub> atmospheric inversion product (Chevallier, 2017a, b) with a horizontal resolution of  $3.75^\circ \times 1.90^\circ$  (longitude  $\times$  latitude) and 39 vertical levels between the surface and the tropopause.

## 4 Results

### 4.1 Time series and general statistics

The continuous CO<sub>2</sub> concentration measurement network in the IdF region provides an invaluable opportunity for model validation and data interpretation. In this work, the correlation coefficient, root-mean-square error (RMSE), and mean bias error (MBE) metrics are first used to compare the performance of the WRF-Chem model with respect to the observed CO<sub>2</sub> concentrations from both the GreenLITE™ laser system and in situ continuous stations. In order to compare them with the GreenLITE™ measurements, the modeling results are sampled and integrated along the chord lines, accounting for their positions and heights. For the in situ point measurements, we simply use the CO<sub>2</sub> values from the 1 km WRF-Chem grid cell that contains the observation location.

Table 3, together with Table S2 and Fig. S6, shows the statistics of all the hourly differences between the observed and modeled CO<sub>2</sub> concentrations and the hourly afternoon differences (11:00–16:00 UTC), from December 2015 to November 2016 using the two model configurations (UCM, BEP). The results presented in the Taylor diagrams (Fig. S6) are based on the full year of data and the seasonal statistics are summarized in Table 3. In general, the model performance is better during the afternoon, in terms of both correlation and RMSE, than it is for the full day. These results are consistent with previous findings that show the model has little skill at reproducing the CO<sub>2</sub> fields during the nighttime due to poor representation of vertical mixing during nighttime conditions and in the morning due to inadequate depiction of PBL growth (e.g., Bréon et al., 2015; Boon et al. 2016). Given the better performance of the WRF-Chem model in the afternoon, we focus the following analyses on



CO<sub>2</sub> concentrations acquired during this period of the day only.

The other significant feature is that the UCM scheme shows a large positive bias (8.7–19.6 ppm) with respect to the observations within the city during autumn and winter. In contrast, the statistics for the BEP scheme compared to the observations are significantly better with clear improvements in the correlation and substantial decreases in both the RMSE and MBE. It is well known that the lower part of the atmosphere is, on average, more stable in winter than in summer (Gates, 1961). As a consequence, a significant fraction of the emitted CO<sub>2</sub> remains close to the surface, so that its atmospheric concentrations are, in winter, highly sensitive to local fluxes and variations in vertical mixing, especially in the complex urban areas. The statistics are highly dependent on the choice of the urban canopy scheme, which strongly suggests that the large UCM model–measurement mismatches in winter are linked to difficulties in modeling the vertical mixing within the urban canopy. It is worth noting that CO<sub>2</sub> concentrations are better reproduced by both UCM and BEP in the spring, with correlations that fluctuate between 0.51 and 0.82 across stations. Both urban canopy schemes show lower correlations during summer (0.45–0.63). These lower values are mostly due to the smaller variability of the concentration rather than a higher measurement–model mismatch. Moreover, the UCM and BEP also have comparable performances at peri-urban areas, while the BEP is slightly better at some suburban sites as shown by the statistics. The smallest errors (both in terms of RMSE and bias) are found at Saclay with a measurement inlet that is well above the sources at 100 m a.g.l. (SAC100).

The statistics shown in Table 3, Table S2, and Fig. S6 also indicate the ability of the models to reproduce the CO<sub>2</sub> at two urban in situ stations (JUS & CDS) and the GreenLITE™ measurements. As for the GreenLITE™ data, we first compute the hourly averages of the observed and modeled CO<sub>2</sub> concentrations over all 15 chords for each transceiver (T1 and T2) and then calculate the respective statistics. In general, the model performance is similar for the two types of urban measurements, whereas the performance for urban measurements is slightly inferior to that of the suburban (both in terms of RMSE and correlation). The correlations with observations are better for T1 and T2 than for the two urban in situ sites, which may be due to the fact that T1 and T2 represent an average over a wide area. Therefore, the GreenLITE™ data are less sensitive to local unresolved sources than the in situ measurements. The RMSE with the BEP scheme is within the range of 4.5 to 9.6 ppm for T1, which is substantially superior to those of JUS and CDS, with only one exception at CDS during summer when the value is slightly better for CDS than for T1. In terms of the MBE, the values of T1 are similar to those of CDS, while the BEP simulation reveals an underestimation of CO<sub>2</sub> for T2 and JUS, with a negative bias of up to 5.2 ppm.

Figure S7 shows time series of modeled CO<sub>2</sub> against daily afternoon mean GreenLITE™ observations (11:00–16:00 UTC). Again, it clearly illustrates that the UCM scheme overestimates the CO<sub>2</sub> concentrations close to the surface within the city during winter. The BEP scheme effectively reproduces the seasonal cycle, as well as most synoptic variations in the atmospheric CO<sub>2</sub> measurements. Note that the UCM model–observation discrepancies for T2 are much smaller than those of T1 as the transceiver T2 is 36.5 m higher in altitude, whereas such a difference in modeled CO<sub>2</sub> between T1 and T2 is not obvious for the BEP scheme.

## 4.2 Analyze covariations in CO<sub>2</sub> spatial difference with wind

In this section, we analyze the spatial variations in the CO<sub>2</sub> concentrations that are (i) measured at the in situ stations, (ii) provided by the GreenLITE™ system, and (iii) simulated by the WRF-Chem model. The analysis of spatial differences rather than individual values should strongly reduce the signature of the large-scale pattern due to boundary conditions and better highlight that of the Paris emissions (Bréon et al., 2015). This makes it possible to further evaluate some characteristics of the model and the measurement data.

### 4.2.1 In situ measurement

We analyze the horizontal differences between pairs of in situ stations as a function of wind speed and direction, expecting a larger concentration at the downwind station with respect to the upwind station, in this region of high emission. For wind fields, we use the ECMWF high-resolution operational forecasts (HRES) linearly interpolated at the hourly resolution and extracted at a height of around 25 m a.g.l. (<https://www.ecmwf.int/en/forecasts/datasets/set-i>, last access: 12 November 2019) as a proxy for all stations located within the IdF region. The HRES wind product is used here for two reasons: firstly, our previous study has shown that the wind speeds provided by HRES are, in general, closer to the observations than those provided by WRF (Lian et al., 2018). Secondly, the WRF-Chem model was run with two configurations (UCM and BEP urban canopy schemes) in this study. If we make use of the modeled winds, the UCM and BEP modeled CO<sub>2</sub> spatial differences should be analyzed using their corresponding modeled wind fields, and the observed winds are then needed for the analysis of the observed CO<sub>2</sub> spatial differences. However, given the small-scale wind variations reproduced by the model, it is hard to determine from which station the wind data used in the analysis should come. For the purpose of a fair and uniform comparison, we thus use an independent wind product. Furthermore, the hourly afternoon CO<sub>2</sub> data are classified into the wind classes with a bin width of 1 m s<sup>-1</sup> for wind speed and 11.25° for wind direction. Figure 5 shows the patterns of the observed and modeled CO<sub>2</sub> concentration differences between pairs of in situ

**Table 3.** Seasonal statistics for observed and modeled hourly afternoon CO<sub>2</sub> concentrations for two urban canopy schemes (UCM, BEP) from December 2015 to November 2016. DJF denotes December–January–February, MAM denotes March–April–May, JJA denotes June–July–August, and SON denotes September–October–November. The color highlights the value in the cell, with the minimum in blue, the median in white, and the maximum in red. All other cells are colored proportionally.

(a) Correlation coefficient													
		T1		T2		JUS 30m		CDS 34m		SAC 15m		SAC 100m	
		UCM	BEP	UCM	BEP	UCM	BEP	UCM	BEP	UCM	BEP	UCM	BEP
Hourly afternoon (11–16 UTC)	DJF	0.79	0.83	0.70	0.79	0.68	0.65	0.65	0.59	0.65	0.86	0.65	0.86
	MAM	0.67	0.81	0.69	0.79	0.51	0.60	0.71	0.78	0.77	0.81	0.81	0.82
	JJA	0.46	0.47	0.45	0.46	NA	NA	0.52	0.55	0.57	0.63	0.49	0.49
	SON	0.73	0.83	0.71	0.82	0.55	0.73	0.65	0.75	0.77	0.83	0.74	0.82

(b) Root-mean-square error (RMSE. Unit: ppm)													
		T1		T2		JUS 30m		CDS 34m		SAC 15m		SAC 100m	
		UCM	BEP	UCM	BEP	UCM	BEP	UCM	BEP	UCM	BEP	UCM	BEP
Hourly afternoon (11–16 UTC)	DJF	31.82	5.98	23.79	6.68	42.31	10.08	33.75	9.61	8.14	5.33	7.08	4.92
	MAM	7.84	4.47	6.69	5.12	9.17	6.11	7.27	4.79	5.75	4.55	5.11	4.47
	JJA	7.07	5.99	7.51	7.25	NA	NA	7.26	5.46	5.86	4.06	5.04	4.56
	SON	31.87	9.57	28.39	10.45	42.50	13.09	32.29	12.01	9.72	6.50	8.20	6.46

(c) Mean bias error (MBE. Unit: ppm)													
		T1		T2		JUS 30m		CDS 34m		SAC 15m		SAC 100m	
		UCM	BEP	UCM	BEP	UCM	BEP	UCM	BEP	UCM	BEP	UCM	BEP
Hourly afternoon (11–16 UTC)	DJF	17.37	0.99	12.99	-0.90	13.55	-5.24	19.61	2.69	3.51	1.74	0.59	0.21
	MAM	2.59	0.59	-0.72	-2.71	0.58	-2.36	2.91	0.52	3.22	1.59	2.08	0.46
	JJA	0.66	-0.89	-2.65	-4.09	NA	NA	1.85	0.06	3.14	1.62	1.13	0.17
	SON	14.01	-0.86	8.65	-4.36	12.84	-4.47	11.29	-0.92	4.88	1.14	2.60	0.02

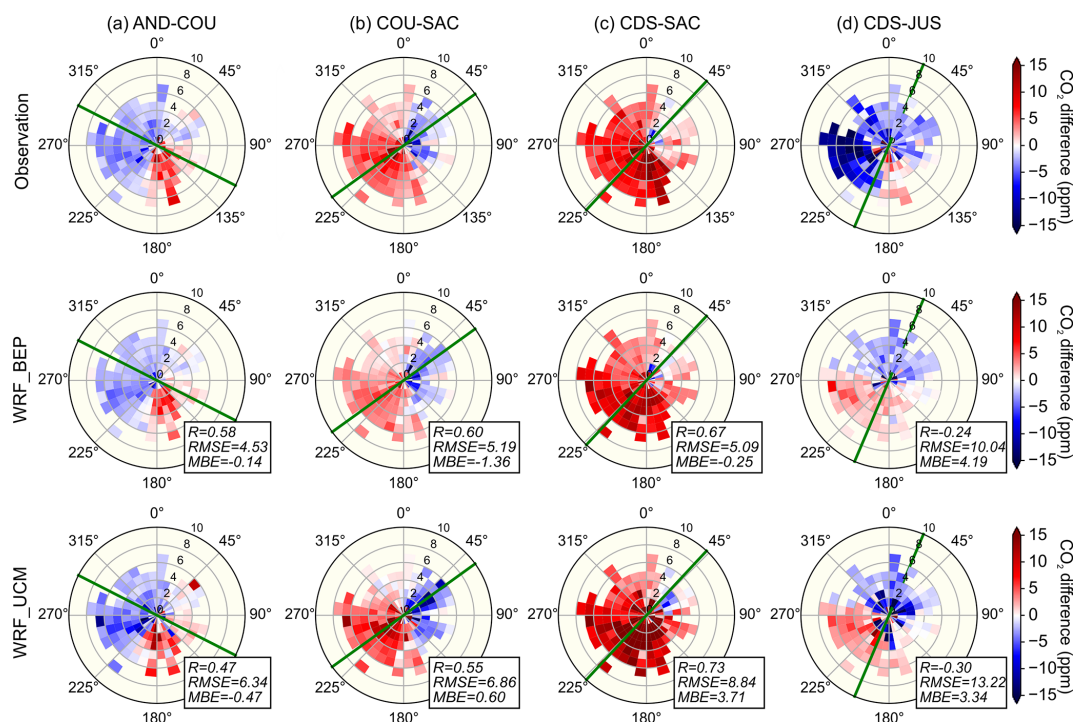
stations, averaged accounting for the wind classes. The standard deviations of CO<sub>2</sub> concentration differences for each wind class are shown in Fig. S8.

Figure 5a shows the observed and modeled CO<sub>2</sub> horizontal differences between AND and COU, two suburban stations located to the north of the city of Paris. One expects that stations downwind of sources of emissions would have a higher CO<sub>2</sub> concentration than those upwind so that the sign of the difference should vary with the wind direction. For this pair of sites (AND and COU), both the model and observations show the expected pattern with a similar amplitude. The values of RMSE and MBE are 4.53 and -0.14 ppm, respectively, for the BEP scheme, implying a slightly better performance than the UCM scheme (6.34 and -0.47 ppm, respectively).

Figure 5b and c show similar figures but for the CO<sub>2</sub> differences between (COU–SAC) and (CDS–SAC). The city of Paris is located between both pairs of stations when the wind is roughly from the northeast or from the southwest directions. Both COU and SAC are located outside of the city and show a pattern with fairly symmetric positive and negative values. Conversely, CDS is in the city of Paris, within an urban environment, and is strongly affected by significant

urban emissions from its surroundings. As a consequence, the CDS–SAC differences in concentration are mostly positive for all wind sectors, with the exception of very specific wind conditions (low winds in the 45° northeast sector). The wind speed also has a strong influence on the differences. The CO<sub>2</sub> difference signal and its variability are generally larger for smaller wind speeds. The model plots (second and third rows) illustrate that the models reproduce the expected cross-city upwind–downwind differences in CO<sub>2</sub> concentrations well. In term of signal amplitude, the BEP scheme is also in better agreement with the observations than the UCM scheme, which is particularly true for the standard deviations shown in Fig. S8.

Conversely, both urban canopy schemes fail to reproduce the wind-related pattern of the observed CDS–JUS difference (Fig. 5d). These observed differences do not show any upwind–downwind patterns and are mostly negative, which can be expected since JUS is close to the city center where strong emissions impact the concentration, whereas CDS is in the middle of a park and is therefore less affected by emissions from its surroundings. The model pattern is dominated by the simple upwind–downwind structure, and it is very much different from the observed values, especially when



**Figure 5.** Spatial differences in CO<sub>2</sub> concentration between two stations of the in situ network, averaged over sets of situation corresponding to bins of wind speed and direction. Only the afternoon (11:00–16:00 UTC) data are used. The top row shows the observations, whereas the other two rows show the two simulations (UCM, BEP). The green line indicates the direction defined by two in situ stations. The statistics of hourly values of observed and modeled CO<sub>2</sub> concentration differences are shown in the box.

the winds are from the west to southwest, where the model values are positive and the observed differences are strongly negative. This model–measurement discrepancy is likely the result of a poor description of the emissions in the city center that are not well reproduced by the 1 km resolution inventory with periodic temporal profiles. It may also indicate that the complex urban structure and morphology, such as buildings and street canyons, affect the energy budget and atmospheric transport, all of which lead to fine-scale (sub-kilometer) CO<sub>2</sub> concentration features that cannot be captured by the WRF-Chem model at a 1 km horizontal resolution. The in situ point measurement may then not be representative of the average within the larger area (1 km<sup>2</sup>) that is simulated by the model.

The analysis of the in situ point measurement differences within and around Paris, together with the simulations, indicates that the model reproduces both the general structure and the amplitude of the cross-city differences in CO<sub>2</sub> concentrations and the CO<sub>2</sub> difference in the Paris surroundings but that it fails to simulate CO<sub>2</sub> differences between the two stations located in the inner city.

#### 4.2.2 GreenLITE<sup>TM</sup> measurement

One expects that the GreenLITE<sup>TM</sup> principle, that provides averaged CO<sub>2</sub> concentrations along the chord lines, is less affected by the local unresolved sources of CO<sub>2</sub> emissions than

the in situ point measurements. Meanwhile, the wide spatial coverage of the GreenLITE<sup>TM</sup> system is expected to provide additional information about CO<sub>2</sub> spatial variations within the city of Paris. In this section, we focus on the spatial variation in CO<sub>2</sub> concentration measured with the GreenLITE<sup>TM</sup> system. As a first step, we analyze the distribution of the absolute values of the observed hourly afternoon CO<sub>2</sub> difference between all pairs of chords for each month together with their simulated counterparts shown in Fig. 6.

We first focus on the winter period (December to February). During that period, the median value of the measured T1 inter-chord range is mostly on the order of 2 ppm. That of T2 is somewhat larger, on the order of 3–4 ppm with some excursions up to 9 ppm. The two simulations with UCM and BEP show very large differences. Whereas BEP simulates spatial variations that are of the right order of magnitude compared to the GreenLITE<sup>TM</sup> data, those of UCM are much larger. Thus, the GreenLITE<sup>TM</sup> measurements provide clear information that favors the BEP over the UCM. During the winter period, there is little vertical mixing, which leads to large vertical gradients in CO<sub>2</sub> concentrations close to the surface. The two simulations differ in their representations of this mixing, which leads to large differences in the modeled CO<sub>2</sub> concentrations. Figure S9 shows that the UCM scheme reproduces a much larger vertical gradient in CO<sub>2</sub> concentrations close to the surface, a few tens of meters above the

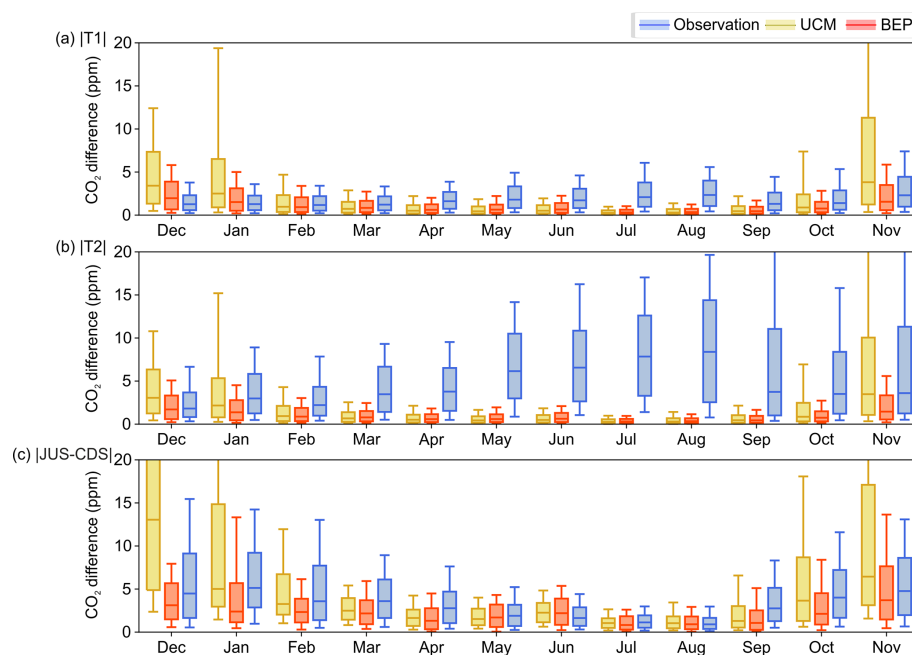


**Figure 6.** Distribution of the GreenLITE<sup>TM</sup> observed and modeled absolute CO<sub>2</sub> concentration differences between all pairs of chords for (a) T1 and (b) T2 from December 2015 to November 2016. (c) Distribution of the observed and modeled absolute CO<sub>2</sub> concentration differences between JUS and CDS from December 2015 to December 2018. The midpoint, the box, and the whiskers represent the 0.5 quantile, 0.25/0.75 quantiles, and 0.1/0.9 quantiles, respectively. Note that only the afternoon data (11:00–16:00 UTC) are used in the analysis.

emissions than the BEP scheme does during the afternoon (11:00–16:00 UTC). The differences are not as large higher up; neither are they further downwind of the emissions as the vertical gradient is then smoother as a result of mixing.

During the summer period, solar insulation generates more instability and the convection generates vertical mixing that limits the horizontal gradients. Both simulations indicate an inter-chord range of less than a few parts per million. Conversely, the GreenLITE<sup>TM</sup> data indicate much larger values, of 3–4 ppm (the median) for T1 and even larger for T2. Further analysis indicates that this spatial variation is mostly systematic, i.e., that some chords are consistently lower or higher than the in situ values. At this point, there are three hypotheses.

- H1: the spatial differences of T1 and T2 are true features linked to fine-scale spatial variations in the emissions between the west and east part of Paris that are under-represented or not included in the emission inventory.
- H2: the models fail in the description of CO<sub>2</sub> concentrations within the city of Paris because of imperfect representations of atmospheric transport processes, excluding inaccuracies in emissions.
- H3: there is a chord-dependent bias in some of the GreenLITE<sup>TM</sup> chords during the summer period.

To resolve this question, we look at the spatial difference between the in situ sites within the city (JUS-CDS) during

summer. Unfortunately, the JUS instrument was not working during the summer of 2016. Therefore, we use the JUS and CDS data over the summers from December 2015 to December 2018 (Fig. 6c). In general, the modeled CO<sub>2</sub> concentration differences between pairs of in situ stations are larger than the modeled inter-chord range of the GreenLITE<sup>TM</sup> system. During the summer, the observed absolute differences between JUS and CDS are only of a few parts per million (the median is on the order of 2 ppm during July and August). These observations indicate that the spatial differences of CO<sub>2</sub> between these two sites within the city of Paris are much smaller during the summer than during the winter and tend to support the modeling results, which would undermine the hypotheses H1 and H2. However, these two stations do not sample the western part of Paris, which is less densely populated with a higher fraction of green areas. The in situ observations do not fully rule out, therefore, the possibility of an impact of the emission spatial structure.

Another potential source of measurement–model discrepancy is the atmospheric transport modeling as proposed in H2. According to previous studies (e.g., Hu et al., 2010), the turbulent eddies and thermals are unlikely to be reproduced properly by the local closure MYJ PBL scheme, which results in insufficient vertical mixing under convective (unstable) conditions, i.e., during summer. It may also indicate that the WRF-Chem model at a 1 km horizontal resolution cannot reproduce the fine-scale (sub-kilometer) CO<sub>2</sub> concentration features over a complex urban environment in Paris,

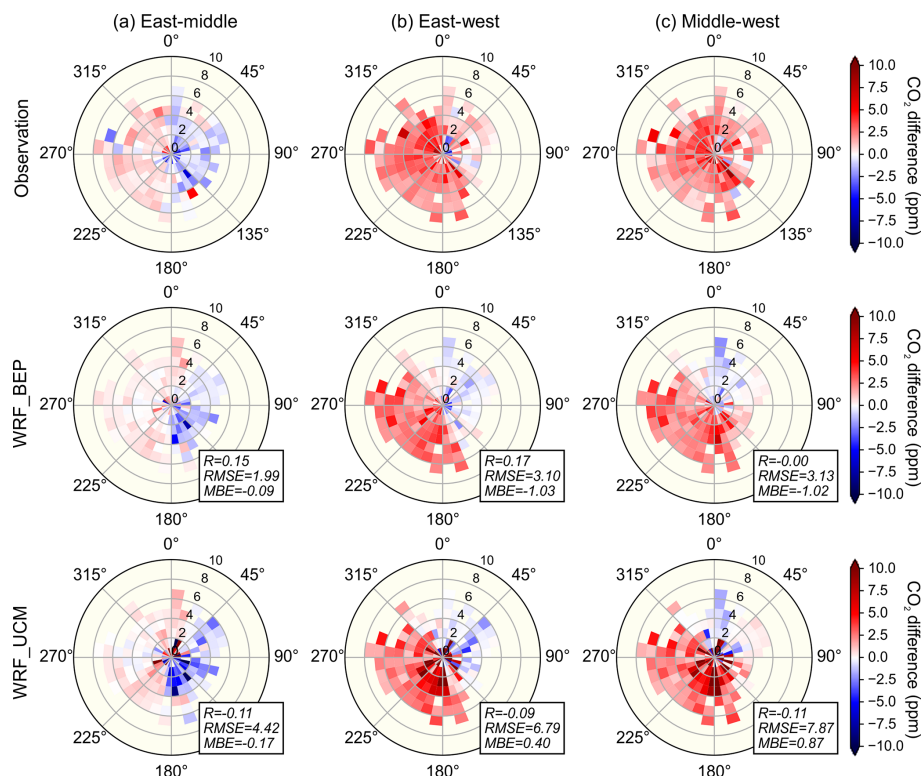


**Figure 7.** Spatial differences in CO<sub>2</sub> concentration between (a) east–middle, (b) east–west, and (c) middle–west parts of the GreenLITE<sup>TM</sup> T1 measurement, averaged accounting for wind speed and direction. Only the afternoon (11:00–16:00 UTC) data are used. The top row shows the observations, whereas the other two rows show the two simulations (UCM, BEP). The statistics of hourly values of observed and modeled CO<sub>2</sub> concentration difference are shown in the box.

as the analysis of JUS and CDS in situ measurements has shown in Sect. 4.2.1.

Atmospheric transport simulations make it possible to assess the respective contributions of various areas/sectors to the measurements. Our preliminary sensitivity experiments (see Figs. S10 and S11 for details) have shown that the anthropogenic emission from the Greater Paris area is the dominant contribution ( $\sim 80\%$ ) to the anthropogenic CO<sub>2</sub> signal at the urban measurement stations. In order to get further insights into the characteristics of CO<sub>2</sub> spatial variations within the city of Paris, it is therefore necessary to analyze the CO<sub>2</sub> differences with the consideration of the anthropogenic CO<sub>2</sub> emissions shown in Figs. 2 and 3. We thus group the 15 chords from T1 into three bins according to both their geographic locations and the amounts of anthropogenic CO<sub>2</sub> emissions averaged along the chords: the western, middle, and eastern parts consist of reflectors R01–R03, reflectors R06–R08, and reflectors R13–R15, respectively, overlying three different regions within Paris. Figure 7 shows the covariations in the GreenLITE<sup>TM</sup> observed and modeled CO<sub>2</sub> spatial difference with winds. The standard deviations of CO<sub>2</sub> concentration differences for each wind class are shown in Fig. S12.

In Fig. 7b and c, we show the east–west and the middle–west differences, where the CO<sub>2</sub> anthropogenic emissions in the western part are systematically lower than the other two regions and the observed CO<sub>2</sub> concentrations in the middle and east are on average higher than in the west. The patterns of observed CO<sub>2</sub> difference are characterized by positive values no matter where the wind blows. The CO<sub>2</sub> differences reproduced by the model are positive in the southwest direction; however, it shows a nearly opposite pattern with those from observations when the wind is from the north-east. A plausible explanation for this is that the influence of kilometer-scale anthropogenic emissions over different parts of Paris on the observed CO<sub>2</sub> concentration has a greater effect than the atmospheric transport and dispersion of the fluxes over the period of study.

Figure 7a shows similar figures but for the east–middle difference. There is a better measurement–model agreement than for Fig. 7b and c. Indeed, as expected, the spatial variations in CO<sub>2</sub> concentrations show negative values over up-wind directions and positive values over downwind directions both for the observation and the model. According to the inventory, the two Paris areas that are covered by the set of chords used here have similar anthropogenic emissions. As a consequence, the overall CO<sub>2</sub> concentration difference,



as shown in Fig. 7a, is then better linked to the impact of atmospheric transport.

We therefore conclude that the pattern of CO<sub>2</sub> concentration differences is consistent with winds only over the areas with similar anthropogenic emissions. In other words, if we compare the CO<sub>2</sub> concentrations of the chords overlaying different level of emissions, the model may be insufficient in accurately modulating the dispersion of CO<sub>2</sub> emissions, the ventilation, and dilution effects at such a high urban microscale resolution.

## 5 Summary and conclusions

In this study, we use conventional in situ measurements together with novel GreenLITE<sup>TM</sup> laser ones for an analysis of the temporal and spatial variations in the CO<sub>2</sub> concentrations within the city of Paris and its vicinity. The analysis also uses 1 km resolution WRF-Chem model coupled with two urban canopy schemes, for the 1-year period from December 2015 to November 2016.

Results show that two urban canopy schemes (UCM, BEP) as part of the WRF-Chem model show similar performances in the areas surrounding the city. They are capable of reproducing the seasonal cycle and most of the synoptic variations in the atmospheric CO<sub>2</sub> in situ measurements over the suburban areas, as well as the general corresponding spatial differences in CO<sub>2</sub> concentration between pairs of in situ stations that span the urban area.

Within the city, these results show very distinct features during winter and summer:

- During the winter, the emissions within the city are the highest, mainly due to household heating, and the vertical mixing is low. This combination leads to large temporal, vertical, and horizontal variations in CO<sub>2</sub> concentrations. The GreenLITE<sup>TM</sup> measurements are less sensitive to local unresolved sources than the in situ point measurements, and are then better suited for the comparison to kilometer-scale modeling. In our analysis, the GreenLITE<sup>TM</sup> data are used to clearly demonstrate that the BEP scheme provides a much better description of the CO<sub>2</sub> fields within the city than the UCM scheme does.
- During the summer, the emissions are lower (by a factor of roughly 2 compared to the cold season) and the sun-induced convection makes the vertical mixing much faster than in winter. For this period, both the in situ measurements and the modeling indicate that, during the afternoon, the spatial differences are limited to a few parts per million. Much larger spatial differences are indicated by the GreenLITE<sup>TM</sup> system, with systematic east–west variations. Although it is not yet fully understood, several pieces of evidence suggest an increase in measurement noise and bias in some of the

GreenLITE<sup>TM</sup> chords during the summer season, that must be resolved or reduced before assimilating the whole data set into the CO<sub>2</sub> atmospheric inversion system that aims at retrieving urban fluxes.

This study stresses the difficulty in reproducing precisely the atmospheric CO<sub>2</sub> concentration within the city because of our inability to represent the detailed spatial structure of the emission and because of the sensitivity of the CO<sub>2</sub> concentration to the strength of vertical mixing. There are strong indications that the uncertainty in the vertical mixing is much larger than the uncertainty in the emissions so that atmospheric concentration measurements within the city can hardly be used to constrain the emission inventories.

*Code and data availability.* All data sets and model results corresponding to this study are available upon request from the corresponding author.

*Supplement.* The supplement related to this article is available online at: <https://doi.org/10.5194/acp-19-13809-2019-supplement>.

*Author contributions.* JL, FMB, GB, and PC contributed to the design and implementation of the research. JL, FMB, GB, PC, TSZ, and JD contributed to the analysis and interpretation of the results. TSZ, JD, MR, and IXR performed the measurements. JS and DS contributed to model input preparation. JL and FMB took the lead in writing the paper with input from all authors.

*Competing interests.* The authors declare that they have no conflict of interest.

*Acknowledgements.* We would like to thank Harris Corporation and the management of Atmospheric and Environmental Research, Inc. for their support of these ongoing analyses. We acknowledge the support of Francois Ravetta (LATMOS/IPSL) and Sorbonne University, for the installation of the GreenLITE<sup>TM</sup> system on the Jussieu Campus. Thanks also to Paris Habitat, Elogie, and Montparnasse ICADE for providing the locations to install the transceivers and reflectors. Finally, thanks to Marc Jamous at Cité des Sciences et de l'Industrie (CDS), to Cristelle Cailteau-Fischbach (LATMOS/IPSL), to OVSQ, and to LSCE/RAMCES technical staff for the maintenance of the in situ monitoring network, coordinated by Delphine Combaz.

*Financial support.* This research has been supported by the IDEX Paris-Saclay (grant no. ANR-11-IDEX-0003-02) together with Harris Corporation.

*Review statement.* This paper was edited by Rob MacKenzie and reviewed by three anonymous referees.

## References

- Ahmadov, R., Gerbig, C., Kretschmer, R., Koerner, S., Neininger, B., Dolman, A. J., and Sarrat, C.: Mesoscale covariance of transport and CO<sub>2</sub> fluxes: Evidence from observations and simulations using the WRF-VPRM coupled atmosphere–biosphere model, *J. Geophys. Res.-Atmos.*, 112, D22107, <https://doi.org/10.1029/2007JD008552>, 2007.
- Ahmadov, R., Gerbig, C., Kretschmer, R., Körner, S., Rödenbeck, C., Bousquet, P., and Ramonet, M.: Comparing high resolution WRF-VPRM simulations and two global CO<sub>2</sub> transport models with coastal tower measurements of CO<sub>2</sub>, *Biogeosciences*, 6, 807–817, <https://doi.org/10.5194/bg-6-807-2009>, 2009.
- AIRPARIF: Bilan des émissions de polluants atmosphériques et de gaz à effet de serre en Île-de-France pour l'année 2010 et historique 2000/2005, available at: [http://www.airparif.asso.fr/\\_pdf/publications/inventaire-emissions-idf-2010-rapport-130731.pdf](http://www.airparif.asso.fr/_pdf/publications/inventaire-emissions-idf-2010-rapport-130731.pdf) (last access: 20 April 2019), 2013.
- Arzoumanian, E., Vogel, F. R., Bastos, A., Gaynullin, B., Laurent, O., Ramonet, M., and Ciais, P.: Characterization of a commercial lower-cost medium-precision non-dispersive infrared sensor for atmospheric CO<sub>2</sub> monitoring in urban areas, *Atmos. Meas. Tech.*, 12, 2665–2677, <https://doi.org/10.5194/amt-12-2665-2019>, 2019.
- Berrisford, P., Dee, D., Poli, P., Brugge, R., Fielding, K., Fuentes, M., Kallberg, P., Kobayashi, S., Uppala, S., and Simmons, A.: The ERA-Interim archive, version 2.0, in: ERA Report Series 1, ECMWF, Shinfield Park, Reading, 2011.
- Boon, A., Broquet, G., Clifford, D. J., Chevallier, F., Butterfield, D. M., Pison, I., Ramonet, M., Paris, J.-D., and Ciais, P.: Analysis of the potential of near-ground measurements of CO<sub>2</sub> and CH<sub>4</sub> in London, UK, for the monitoring of city-scale emissions using an atmospheric transport model, *Atmos. Chem. Phys.*, 16, 6735–6756, <https://doi.org/10.5194/acp-16-6735-2016>, 2016.
- Bréon, F. M., Broquet, G., Puygrenier, V., Chevallier, F., Xueref-Remy, I., Ramonet, M., Dieudonné, E., Lopez, M., Schmidt, M., Perrussel, O., and Ciais, P.: An attempt at estimating Paris area CO<sub>2</sub> emissions from atmospheric concentration measurements, *Atmos. Chem. Phys.*, 15, 1707–1724, <https://doi.org/10.5194/acp-15-1707-2015>, 2015.
- Buchwitz, M.: Copernicus Sentinel Kandidat CO<sub>2</sub> Monitoring (CO2M) Mission, oral (and poster) presentation given at Nationales Forum fuer Fernerkundung und Copernicus 2018 “Copernicus gestaltet”, Bundesministerium fuer Verkehr und digitale Infrastruktur, 27–29 November 2018, Berlin, 2018.
- Chen, F. and Dudhia, J.: Coupling an advanced land surface-hydrology model with the Penn State-NCAR MM5 modeling system. Part I: Model implementation and sensitivity, *Mon. Weather Rev.*, 129, 569–585, 2001.
- Chen, F., Kusaka, H., Bornstein, R., Ching, J., Grimmond, C. S. B., Grossman-Clarke, S., Loridan, T., Manning, K. W., Martilli, A., Miao, S., Sailor, D., Salamanca, F. P., Taha, H., Tewari, M., Wang, X., Wyszogrodzki, A. A., and Zhang, C.: The integrated WRF/urban modelling system: development, evaluation, and applications to urban environmental problems, *Int. J. Climatol.*, 31, 273–288, 2011.
- Chevallier, F.: Description of the CO<sub>2</sub> inversion production chain. CAMS deliverable CAMS73\_2015SC2\_D73.1.5.5\_201703\_CO2 inversion production chain\_v1, available at: <http://atmosphere.copernicus.eu/> (last access: 12 November 2019), 2017a.
- Chevallier, F.: Validation report for the inverted CO<sub>2</sub> fluxes, v16r1. CAMS deliverable CAMS73\_2015SC2\_D73.1.4.2-1979-2016-v1\_201707, available at: <http://atmosphere.copernicus.eu/> (last access: 12 November 2019), 2017b.
- Clough, S. A., Shephard, M. W., Mlawer, E. J., Delamere, J. S., Iacono, M. J., Cady-Pereira, K., Boukabara, S., and Brown, P. D.: Atmospheric radiative transfer modeling: a summary of the AER codes, *Short Communication, J. Quant. Spectrosc. Ra.*, 91, 233–244, 2005.
- Crisp, D.: Measuring atmospheric carbon dioxide from space with the Orbiting Carbon Observatory-2 (OCO-2), in: *Earth Observing Systems XX*, Int. Soc. Optics Photon., 9607, 960702, 2015.
- Crisp, D., Miller, C. E., and DeCola, P. L.: NASA Orbiting Carbon Observatory: measuring the column averaged carbon dioxide mole fraction from space, *J. Appl. Remote Sens.*, 2, 23508, <https://doi.org/10.1117/1.2898457>, 2008.
- Davis, K. J., Deng, A., Lauvaux, T., Miles, N. L., Richardson, S. J., Sarmiento, D. P., Gurney, K. R., Hardesty, R. M., Bonin, T. A., Brewer, W. A., Lamb, B. K., Shepson, P. B., Harvey, R. M., Cambaliza, M. O., Sweeney, C., Turnbull, J. C., Whetstone, J., and Karion, A.: The Indianapolis Flux Experiment (INFLUX): A test-bed for developing urban greenhouse gas emission measurements, *Elem. Sci. Anth.*, 5, 21, <https://doi.org/10.1525/elementa.188>, 2017.
- Deng, A., Lauvaux, T., Davis, K. J., Gaudet, B. J., Miles, N., Richardson, S. J., Wu, K., Sarmiento, D. P., Hardesty, R. M., Bonin, T. A., Brewer, W. A., and Gurney, K. R.: Toward reduced transport errors in a high resolution urban CO<sub>2</sub> inversion system, *Elem. Sci. Anth.*, 5, 20, <https://doi.org/10.1525/elementa.133>, 2017.
- Dobler, J. T., Harrison, F. W., Browell, E. V., Lin, B., McGregor, D., Kooi, S., Choi, Y., and Ismail, S.: Atmospheric CO<sub>2</sub> column measurements with an airborne intensity-modulated continuous wave 1.57  $\mu$ m fiber laser lidar, *Appl. Optics*, 52, 2874–2892, 2013.
- Dobler, J. T., Zaccheo, T. S., Pernini, T. G., Blume, N., Broquet, G., Vogel, F., Ramonet, M., Braun, M., Stauffer, J., Ciais, P., and Botos, C.: Demonstration of spatial greenhouse gas mapping using laser absorption spectrometers on local scales, *J. Appl. Remote Sens.*, 11, 014002, <https://doi.org/10.1117/1.JRS.11.014002>, 2017.
- Dudhia, J.: Numerical study of convection observed during the winter monsoon experiment using a mesoscale two-dimensional model, *J. Atmos. Sci.*, 46, 3077–3107, 1989.
- Duren, R. M. and Miller, C. E.: Measuring the carbon emissions of megacities, *Nat. Clim. Change*, 2, 560–562, 2012.
- Edner, H., Ragnarson, P., Spännare, S., and Svanberg, S.: Differential optical absorption spectroscopy (DOAS) system for urban atmospheric pollution monitoring, *Appl. Optics*, 32, 327–333, 1993.
- Eldering, A., Taylor, T. E., O'Dell, C. W., and Pavlick, R.: The OCO-3 mission: measurement objectives and expected

- performance based on 1 year of simulated data, *Atmos. Meas. Tech.*, 12, 2341–2370, <https://doi.org/10.5194/amt-12-2341-2019>, 2019.
- Feng, S., Lauvaux, T., Newman, S., Rao, P., Ahmadov, R., Deng, A., Díaz-Isaac, L. I., Duren, R. M., Fischer, M. L., Gerbig, C., Gurney, K. R., Huang, J., Jeong, S., Li, Z., Miller, C. E., O’Keeffe, D., Patarasuk, R., Sander, S. P., Song, Y., Wong, K. W., and Yung, Y. L.: Los Angeles megacity: a high-resolution land-atmosphere modelling system for urban CO<sub>2</sub> emissions, *Atmos. Chem. Phys.*, 16, 9019–9045, <https://doi.org/10.5194/acp-16-9019-2016>, 2016.
- Font, A., Grimmond, C. S. B., Kotthaus, S., Morguá, J. A., Stockdale, C., O’Connor, E., Priestman, M., and Barratt, B.: Daytime CO<sub>2</sub> urban surface fluxes from airborne measurements, eddy-covariance observations and emissions inventory in Greater London, *Environ. Poll.*, 196, 98–106, 2015.
- Gates, W. L.: Static stability measures in the atmosphere, *J. Meteorol.*, 18, 526–533, 1961.
- Graven, H. D., Stephens, B. B., Guilderson, T. P., Campos, T. L., Schimel, D. S., Campbell, J. E., and Keeling, R. F.: Vertical profiles of biospheric and fossil fuel-derived CO<sub>2</sub> and fossil fuel CO<sub>2</sub>: CO ratios from airborne measurements of  $\Delta^{14}\text{C}$ , CO<sub>2</sub> and CO above Colorado, USA, *Tellus B*, 61, 536–546, 2009.
- Grell, G. A. and Dévényi, D.: A generalized approach to parameterizing convection combining ensemble and data assimilation techniques, *Geophys. Res. Lett.*, 29, 38-1–38-4, 2002.
- Hamazaki, T., Kaneko, Y., and Kuze, A.: Carbon dioxide monitoring from the GOSAT satellite, in: Proceedings XXth ISPRS conference, 12–23 July 2004, Istanbul, Turkey, p. 3, available at: <http://www.isprs.org/istanbul2004/comm7/papers/43.pdf> (last access: 12 November 2019), 2004.
- Hong, S. Y. and Lim, J. O. J.: The WRF single-moment 6-class microphysics scheme (WSM6), *J. Korean Meteorol. Soc.*, 42, 129–151, 2006.
- Hu, X. M., Nielsen-Gammon, J. W., and Zhang, F.: Evaluation of three planetary boundary layer schemes in the WRF model, *J. Appl. Meteorol. Clim.*, 49, 1831–1844, 2010.
- IEA: World energy outlook, International Energy Agency (IEA), Paris, 2008.
- Janjić, Z. I.: The step-mountain coordinate: Physical package, *Mon. Weather Rev.*, 118, 1429–1443, 1990.
- Janjić, Z. I.: The step-mountain eta coordinate model: Further developments of the convection, viscous sublayer, and turbulence closure schemes, *Mon. Weather Rev.*, 122, 927–945, 1994.
- Janjić, Z. I.: The surface layer in the NCEP Eta Model, in: Eleventh Conference on Numerical Weather Prediction, 19–23 August 1996, Norfolk, VA, American Meteorological Society, Boston, MA, 354–355, 1996.
- Jung, M., Henkel, K., Herold, M., and Churkina, G.: Exploiting synergies of global land cover products for carbon cycle modeling, *Remote Sens. Environ.*, 101, 534–553, 2006.
- Lauvaux, T., Miles, N. L., Deng, A., Richardson, S. J., Cambaliza, M. O., Davis, K. J., Gaudet, B., Gurney, K. R., Huang, J., O’Keeffe, D., Song, Y., Karion, A., Oda, T., Patarasuk, R., Sarmiento, D., Shepson, P., Sweeney, C., Turnbull, J., and Wu, K.: High-resolution atmospheric inversion of urban CO<sub>2</sub> emissions during the dormant season of the Indianapolis Flux Experiment (INFLUX), *J. Geophys. Res.-Atmos.*, 121, 5213–5236, 2016.
- Le Quéré, C., Andrew, R. M., Friedlingstein, P., Sitch, S., Hauck, J., Pongratz, J., Pickers, P. A., Korsbakken, J. I., Peters, G. P., Canadell, J. G., Arneeth, A., Arora, V. K., Barbero, L., Bastos, A., Bopp, L., Chevallier, F., Chini, L. P., Ciais, P., Doney, S. C., Gkritzalis, T., Goll, D. S., Harris, I., Haverd, V., Hoffman, F. M., Hoppema, M., Houghton, R. A., Hurtt, G., Ilyina, T., Jain, A. K., Johannessen, T., Jones, C. D., Kato, E., Keeling, R. F., Goldewijk, K. K., Landschützer, P., Lefèvre, N., Lienert, S., Liu, Z., Lombardozzi, D., Metzl, N., Munro, D. R., Nabel, J. E. M. S., Nakaoka, S., Neill, C., Olsen, A., Ono, T., Patra, P., Peregon, A., Peters, W., Peylin, P., Pfeil, B., Pierrot, D., Poulter, B., Rehder, G., Resplandy, L., Robertson, E., Rocher, M., Rödenbeck, C., Schuster, U., Schwinger, J., Séférian, R., Skjelvan, I., Steinhoff, T., Sutton, A., Tans, P. P., Tian, H., Tilbrook, B., Tubiello, F. N., van der Laan-Luijkx, I. T., van der Werf, G. R., Viovy, N., Walker, A. P., Wiltshire, A. J., Wright, R., Zaehle, S., and Zheng, B.: Global Carbon Budget 2018, *Earth Syst. Sci. Data*, 10, 2141–2194, <https://doi.org/10.5194/essd-10-2141-2018>, 2018.
- Lian, J., Wu, L., Bréon, F. M., Broquet, G., Vautard, R., Zaccaro, T. S., Dobler, J., and Ciais, P.: Evaluation of the WRF-UCM mesoscale model and ECMWF global operational forecasts over the Paris region in the prospect of tracer atmospheric transport modeling, *Elem. Sci. Anth.*, 6, 64, <https://doi.org/10.1525/elementa.319>, 2018.
- Mahadevan, P., Wofsy, S. C., Matross, D. M., Xiao, X., Dunn, A. L., Lin, J. C., Gerbig, C., Munger, J. W., Chow, V. Y., and Gottlieb, E. W.: A satellite-based biosphere parameterization for net ecosystem CO<sub>2</sub> exchange: Vegetation Photosynthesis and Respiration Model (VPRM), *Global Biogeochem. Cy.*, 22, GB2005, <https://doi.org/10.1029/2006GB002735>, 2008.
- Martilli, A., Clappier, A., and Rotach, M. W.: An urban surface exchange parameterisation for mesoscale models, *Bound.-Lay. Meteorol.*, 104, 261–304, 2002.
- Mlawer, E. J., Taubman, S. J., Brown, P. D., Iacono, M. J., and Clough, S. A.: Radiative transfer for inhomogeneous atmospheres: RRTM, a validated correlated-*k* model for the longwave, *J. Geophys. Res.-Atmos.*, 102, 16663–16682, 1997.
- Moore, B., Crowell, S., Rayner, P., Kumer, J., O’Dell, C., O’Brien, D., Utembe, S., Polonsky, I., Schimel, D., and Lemen, J.: The potential of the Geostationary Carbon Cycle Observatory (GeoCarb) to provide multi-scale constraints on the carbon cycle in the Americas, *Front. Environ. Sci.*, 6, 109, <https://doi.org/10.3389/fenvs.2018.00109>, 2018.
- Mueller, K., Yadav, V., Lopez-Coto, I., Karion, A., Gourdji, S., Martin, C., and Whetstone, J.: Siting background towers to characterize incoming air for urban greenhouse gas estimation: a case study in the Washington, DC/Baltimore area, *J. Geophys. Res.-Atmos.*, 123, 2910–2926, 2018.
- Nehrkorn, T., Henderson, J., Leidner, M., Mountain, M., Eluszkiewicz, J., McKain, K., and Wofsy, S.: WRF simulations of the urban circulation in the Salt Lake City area for CO<sub>2</sub> modeling, *J. Appl. Meteorol. Clim.*, 52, 323–340, 2013.
- Salamanca, F., Krpo, A., Martilli, A., and Clappier, A.: A new building energy model coupled with an urban canopy parameterization for urban climate simulations-part I. formulation, verification, and sensitivity analysis of the model, *Theor. Appl. Climatol.*, 99, 331–344, 2010.
- Sargent, M., Barrera, Y., Nehrkorn, T., Hutyla, L. R., Gately, C. K., Jones, T., McKain, K., Sweeney, C., Hegarty, J., Hardiman, B.,

- Wang, J. A., and Wofsy, S. C.: Anthropogenic and biogenic CO<sub>2</sub> fluxes in the Boston urban region, *P. Natl. Acad. Sci. USA*, 115, 7491–7496, 2018.
- Stauffer, J., Broquet, G., Bréon, F.-M., Puygrenier, V., Chevallier, F., Xueref-Rémy, I., Dieudonné, E., Lopez, M., Schmidt, M., Ramonet, M., Perrussel, O., Lac, C., Wu, L., and Ciais, P.: The first 1-year-long estimate of the Paris region fossil fuel CO<sub>2</sub> emissions based on atmospheric inversion, *Atmos. Chem. Phys.*, 16, 14703–14726, <https://doi.org/10.5194/acp-16-14703-2016>, 2016.
- Tans, P., Zhao, C., and Kitzis, D.: The WMO Mole Fraction Scales for CO<sub>2</sub> and other greenhouse gases, and uncertainty of the atmospheric measurements, in: Report of the 15th WMO/IAEA Meeting of Experts on Carbon Dioxide, Other Greenhouse Gases, and Related Tracers Measurement Techniques, 7–10 September 2009, GAW Report No. 194, WMO TD No. 1553, WMO, Jena, Germany, 152–159, 2011.
- Wang, H., Zhang, R., Liu, M., and Bi, J.: The carbon emissions of Chinese cities, *Atmos. Chem. Phys.*, 12, 6197–6206, <https://doi.org/10.5194/acp-12-6197-2012>, 2012.
- Wu, L., Broquet, G., Ciais, P., Bellassen, V., Vogel, F., Chevallier, F., Xueref-Remy, I., and Wang, Y.: What would dense atmospheric observation networks bring to the quantification of city CO<sub>2</sub> emissions?, *Atmos. Chem. Phys.*, 16, 7743–7771, <https://doi.org/10.5194/acp-16-7743-2016>, 2016.
- Xueref-Remy, I., Dieudonné, E., Vuillemin, C., Lopez, M., Lac, C., Schmidt, M., Delmotte, M., Chevallier, F., Ravetta, F., Perrussel, O., Ciais, P., Bréon, F.-M., Broquet, G., Ramonet, M., Spain, T. G., and Ampe, C.: Diurnal, synoptic and seasonal variability of atmospheric CO<sub>2</sub> in the Paris megacity area, *Atmos. Chem. Phys.*, 18, 3335–3362, <https://doi.org/10.5194/acp-18-3335-2018>, 2018.
- Zaccheo, T. S., Blume, N., Pernini, T., Dobler, J., and Lian, J.: Bias correction of long-path CO<sub>2</sub> observations in a complex urban environment for carbon cycle model inter-comparison and data assimilation, *Atmos. Meas. Tech.*, 12, 5791–5800, <https://doi.org/10.5194/amt-12-5791-2019>, 2019.